

## Article

# Host–Guest Inclusion Complexes of Essential Oils with Strong Antibacterial and Antifungal Features in Beta-Cyclodextrin for Solid-State Pharmaceutical Applications

Aldo Arrais <sup>1,\*</sup>, Marta Manzoni <sup>1</sup>, Alessia Cattaneo <sup>1</sup>, Valentina Gianotti <sup>2</sup>, Nadia Massa <sup>2</sup>, Giorgia Novello <sup>2</sup>, Alice Caramaschi <sup>2</sup>, Elisa Gamalero <sup>2</sup> and Elisa Bona <sup>1,\*</sup>

<sup>1</sup> Dipartimento di Scienze e Innovazione Tecnologica, Università del Piemonte Orientale, Piazza San Eusebio 5, 13100 Vercelli, Italy; marta.manzoni@uniupo.it (M.M.); alessia.cattaneo@uniupo.it (A.C.)

<sup>2</sup> Dipartimento di Scienze e Innovazione Tecnologica, Università del Piemonte Orientale, Viale T. Michel 11, 15121 Alessandria, Italy; valentina.gianotti@uniupo.it (V.G.); nadia.massa@uniupo.it (N.M.); giorgia.novello@uniupo.it (G.N.); alice.caramaschi@uniupo.it (A.C.); elisa.gamalero@uniupo.it (E.G.)

\* Correspondence: aldo.arrais@uniupo.it (A.A.); elisa.bona@uniupo.it (E.B.); Tel.: +39-016-122-8357 (E.B.)

**Abstract:** Essential oils are widely recognized as natural alternatives to pharmaceutical antibacterial and antifungal agents. With respect to standard pharmaceuticals, the advantages of essential oils are their (i) low production costs, (ii) lack of chemical and biochemical drawbacks that are intrinsic to the synthetic production process and (iii) good tolerance by humans. On the other hand, the liquid nature of essential oils poses concerns about their actual application in different therapeutic issues regarding their persistence and the ability to control or prolong drug release. In this study, two essential oils from oregano and winter savory showing antibacterial and antifungal features were complexed in a solid state with beta-cyclodextrin. Host–guest inclusion complexes were characterized using FT-IR spectroscopy, ESI-MS and GC-MS techniques. Manyfold terpenic and non-terpenic components of the oils could be observed and unambiguously identified as being included inside the carbohydrate hosts. Many of them provided a specific biocidal action. Indeed, essential oil host–guest inclusion products were tested against two *Candida* species and an *S. aureus* reference strain, showing that the oils effectively maintained their liquid performances. Solid-state tablets of the essential oil inclusion complexes embedded in polyvinylpyrrolidone could be obtained. These results pave the way for the solid-state application of essential oils in antibacterial and antifungal pharmaceutical treatments.

**Keywords:** essential oils; beta-cyclodextrin; host–guest molecular inclusion complexes; solid-state tablet; antibacterial and antifungal performance; *S. aureus*; *Candida* sp.



**Citation:** Arrais, A.; Manzoni, M.; Cattaneo, A.; Gianotti, V.; Massa, N.; Novello, G.; Caramaschi, A.; Gamalero, E.; Bona, E. Host–Guest Inclusion Complexes of Essential Oils with Strong Antibacterial and Antifungal Features in Beta-Cyclodextrin for Solid-State Pharmaceutical Applications. *Appl. Sci.* **2021**, *11*, 6597. <https://doi.org/10.3390/app11146597>

Academic Editors: Adriana Basile, Sergio Sorbo and Viviana Maresca

Received: 6 July 2021

Accepted: 16 July 2021

Published: 18 July 2021

**Publisher's Note:** MDPI stays neutral with regard to jurisdictional claims in published maps and institutional affiliations.



**Copyright:** © 2021 by the authors. Licensee MDPI, Basel, Switzerland. This article is an open access article distributed under the terms and conditions of the Creative Commons Attribution (CC BY) license (<https://creativecommons.org/licenses/by/4.0/>).

## 1. Introduction

As dramatically experienced in the recent world pandemic crisis, viral, bacterial and fungal threats will provide highly serious concerns in the global context of human health in the near future [1,2]. Regarding this specific issue, hard challenges will have to be tackled, both in terms of scientific biomedical research and the socio-political and economical perspectives. Regarding the former, the World Health Organization (WHO) has sponsored and promoted research studies that are aiming at the development of medical features that use natural products [3]. Although they are often competitive with synthetic pharmaceuticals regarding clinical performance, they lack all their main critical drawbacks, i.e., the environmental impact of chemical syntheses and the high economic costs of processes [4,5]. Antibiotics have impacted healthcare since their first introduction approximately 90 years ago. Unfortunately, their excessive use in veterinary and agricultural fields resulted in the tremendous flow of antibiotics into the environment [6,7]. This exposure leads to enormous selective pressures that drive the evolution of antimicrobial resistance genes in pathogenic and commensal bacteria [6,8,9]. Thanks to these antibiotic-resistant genes, bacteria are

able to overcome antibiotic effects in different ways, such as via the use of an efflux pump, enzymatic antibiotic molecule deactivation and chemical modification of their cellular targets [10]. These resistance mechanisms reduced the therapeutical efficacy of antibiotic drugs [9]. The Centers for Disease Control and Prevention reported in 2019 that *S. aureus* and *Candida* sp. are serious threats. In particular, in hospitalized patients in 2017, it was estimated that *S. aureus* led to 323,700 cases and 10,600 deaths, while *Candida* sp. led to 34,800 cases with 1700 deaths [6]. It is also predicted that by the year 2050, drug-resistant pathogens will cause 10 million fatalities per year. This means that drug-resistant pathogens will cause more deaths than traffic accidents, diabetes and cancer [11].

Skin infections caused by *S. aureus* and mucous membrane infections caused by various *Candida* species are widespread and can produce serious problems, especially in immunocompromised individuals. In particular, *S. aureus* is a pathogen that causes skin infections with a wide range of severity, from impetigo to abscesses. *Candida* species emergence is constantly increasing and the most isolated species from oral and vaginal candidiasis are *C. albicans* and *C. glabrata* [12].

The previously described diseases have the characteristic of generally being limited to the site of infection, but they may spread in a disseminated manner within the organism. For this reason, these infections are to be seriously considered for their potential threat.

In the past, plants were employed in traditional medicine for the treatment of several diseases [13]. Essential oils (EOs) are extracted from different plant organs—namely, leaves, flowers, fruits, seeds, roots, buds, stems and wood [14]—and are volatile, complex natural mixtures of organic compounds that are characterized by a strong fragrance. EOs extracted from Mediterranean aromatic plants are usually employed as flavors in food and drinks, as well as in cosmetic and pharmaceutical preparations. Different papers reported their inhibitory activities against fungal and bacterial pathogens [15,16]. EOs with high concentrations of phenols are recognized for their antifungal and antibacterial activities. In particular, EOs extracted from oregano and winter savory are reported to have activity against several microorganisms [17].

The natural EOs' antiseptic performances against bacterial and fungal strains mimic those of antibiotics applied in clinical routine [14–17]. Unfortunately, they have serious limitations in clinical employment as medical devices: their liquid and oily nature. This feature poses intrinsic obstacles in the delivery and prolonged release duration of the antiseptic components of each EO.

Therefore, the aim of this study was to include EOs in beta-cyclodextrins (b-CD), transferring their liquid components in a solid state. Two high-performance EOs extracted from winter savory (*Satureja montana*) and oregano (*Thymus capitatus*), which previously provided excellent antibacterial and antifungal performances against *S. aureus* and different *Candida* strains [16–19], were used. The obtained solid-state natural products were characterized from a chemical point of view and tested for their biological effects. Moreover, the solid-state complexes were pelleted in capsules, which is a prototypal model for clinical administration.

## 2. Materials and Methods

### 2.1. Synthesis of Host–Guest Molecular Inclusion Complexes

All chemical reactants and solvents were purchased from Sigma Adrich (Merck Corp., Schnellerdorf, D) and used as received. *S. montana* and *T. capitatus* EOs were kindly provided by Flora s.r.l. (Pisa, Italy).

The standard synthetic protocol requires a nearly stoichiometric 1:1 mixture of b-CD and EOs, which were mixed together in a 50 mL round flask and sonicated using an Argo-Lab DU-32 sonication bath for 45 min at 45 °C. Detailed parameters for the two investigated EOs were 506 mg of b-CD and 496 mg of the *S. montana* EO, and 499 mg of b-CD and 506 mg of the *T. capitatus* EO. After treatment, the solid-state materials were mechanically separated from the residual oils, set in a 50 mL beaker and washed with 5 mL of deionized water to remove the unreacted b-CD. Washed solids were then dried under reduced pressure in

a ventilated hood. After 72 h, white dried solid powders were obtained. In successively improved syntheses, larger amounts (750–900 mg) of b-CD were applied in the starting mixtures prior to the sonication synthetic treatment in order to also ensure that the potential b-CD–EO 2:1 inclusion complexes for the bigger molecular components were contained in the natural EO formulation. Hence, high quantitative yields of solid-state powder products were obtained.

## 2.2. FT-IR Spectroscopy

Fourier-transform infrared (FT-IR) solid-state spectra were obtained with a Thermo Fisher Scientific Nicolet iS50 spectrophotometer (1 cm diameter KBr disks containing 1–3 mg of the solid-state sample, pressed at 10 Ton per square centimeter; 100 spectral averaged scans at  $2\text{ cm}^{-1}$  spectral resolution). The liquid EOs' spectral patterns were obtained via 1 droplet oil impregnation of a blank KBr disk. The reported and commented spectral profiles were supported by supplementary  $1\text{ cm}^{-1}$  high-resolution FT-IR spectra.

## 2.3. ESI-MS Spectrometry

Mass spectra were recorded using a Finnigan LCQ LTQ spectrometer detector equipped with an electrospray ion source (ESI) and a linear ion trap analyzer. The mass spectra were obtained via direct infusion (flow rate of  $20.0\text{ mL min}^{-1}$ ) in an ESI ion source with  $10.0\text{ mg L}^{-1}$  acetonitrile solutions. The mass spectrometry analyses were performed in positive ion (PI) mode ( $3\text{ }\mu\text{s scans s}^{-1}$ , 50 ms inlet time). The ESI probe tip was set at 4.50 kV and heated capillary at  $270\text{ }^{\circ}\text{C}$ . In positive polarity mode, the capillary potential was set at 3.00 V and ion optics parameters were optimized using the following values: tube lens offset—5.00 V; first octapole voltage—6.00 V; inner octapole lens voltage—26.00 V; second octapole voltage—9.50 V. High-purity nitrogen was used as a nebulizer (sheath and auxiliary gas pressures set at 60 and 20 on the arbitrary scale 0–100 of the instrument, respectively) and helium (>99.999%) served as the quenching agent. Samples were dissolved in acetonitrile and analyzed via direct infusion after filtration (PTFE membrane filters,  $0.22\text{ }\mu\text{m}$ ).

## 2.4. GC-MS Analysis

Chromatographic characterization was performed using a Finnigan Trace GC-Ultra and Trace DSQ. In detail, gas chromatographic separation was obtained using a capillary column Phenomenex DB5-5 ms (30 m,  $0.25\text{ mm i.d.}$ ,  $0.25\text{ }\mu\text{m}$  thickness). The inlet temperature was set to  $250\text{ }^{\circ}\text{C}$  in splitless mode and helium was used as the carrier gas with a constant flow of  $1.0\text{ mL min}^{-1}$ . The initial oven temperature was set to  $70\text{ }^{\circ}\text{C}$  and reached  $250\text{ }^{\circ}\text{C}$  with a constant gradient of  $5\text{ }^{\circ}\text{C min}^{-1}$ . The mass spectrometer (MS) transfer line temperature was set to  $290\text{ }^{\circ}\text{C}$ . The MS signal was acquired through the  $\text{EI}^+$  mode with an ionization energy of 70.0 eV and a source temperature of  $290\text{ }^{\circ}\text{C}$ . The detection was carried out in full-scan mode in the range of 35–500  $m/z$ . The samples were prepared by dissolving oil extracts and the correspondent inclusion complex in diethyl-ether and injected in the GC after a filtration (PTFE membrane filters,  $0.22\text{ }\mu\text{m}$ ).

## 2.5. Synthesis of the Pharmaceutical b-CD–EO Tablet

In a standardized procedure, 15–25 mg of the b-CD–EOs powder mixtures were embedded in 35–45 mg of polyvinylpyrrolidone (PVP) by mixing them in an agate mortar with an agate pestle. The obtained solid-state composite powder was then transferred and pressed for 1 min at  $10\text{ Ton/cm}^2$ , thus obtaining a 1 cm diameter round tablet (5 mm thickness) to be applied in specific plate diffusion tests.

A proto-pharmaceutical formulation of b-CD–EOs embedded in a solid-state tablet was obtained. The actual composition is at present under an Italian patent.

## 2.6. Antifungal and Antibacterial Assays

The agar disk diffusion method was employed to determine the antifungal and antibacterial activity of the free EOs, according to previously published methods [16–20] or complexed in a solid state with b-CD (tablet). The b-CD activity against yeast and bacteria was also tested using the same method.

### 2.6.1. Antifungal Assay

The antifungal assays were carried out with the reference strains *C. albicans* ATCC 14,053 and *C. glabrata* ATCC 15126. The antifungal effects of clotrimazole (10 µg), the EOs and the tablets were evaluated according to Clinical and Laboratory Standards Institute Standard M44-A. Briefly, strain suspensions ( $10^6$  CFU mL<sup>-1</sup>) were swabbed on Mueller-Hinton Agar added with 2% glucose and 0.5 µg/mL Methylene Blue Dye (GMB). A filter paper disk (6 mm diameter) was placed on the agar surface and added with 10 µL of pure EO in order to evaluate its antifungal activity. Moreover, to evaluate the antifungal potential of the produced tablets, the same diffusion assay was performed using the tablet (one of each EO in triplicate) in place of a paper disk. Tablet dissolution was also monitored every five minutes. Clotrimazole (10 µg) disks were used as positive controls. Pure dimethyl sulfoxide (DMSO; Sigma-Aldrich, St. Louis, MO, USA; 10 µL) and organic linseed oil (10 µL) disks were used as negative controls. Plates were incubated at 37 °C for 48 h. All experiments were performed in triplicate. The sensitivity test for the EO was considered positive if it resulted in an inhibition halo that was larger than that induced by clotrimazole (positive control  $\geq$  100%).

### 2.6.2. Antibacterial Assay

The antibacterial assays were carried out with the reference strain *S. aureus* NCTC 6571. Vancomycin's effects were evaluated according to EUCAST Disk Diffusion Method for Antimicrobial Susceptibility v. 7.0 (January 2021). The sensitivity to the EOs was assessed using the agar disk diffusion method: strain suspensions (0.5 McFarland), obtained in physiological solution, were swabbed on Mueller Hinton Agar (Biolife Italiana s.r.l., Milan, Italy) plates. Filter paper disks (6.0 mm diameter) were placed on the agar surface and 10 µL of pure EO was added in order to evaluate its antibacterial activity. Moreover, to evaluate the antimicrobial potential of the produced tablets, the same diffusion assay was performed using the tablet (one of each EO, in triplicate) in place of a paper disk. Tablet dissolution was also monitored every five minutes. Pure dimethyl sulfoxide (DMSO) (D-8418-Sigma-Aldrich, St. Louis, MO, USA) (10 µL) and organic linseed oil (10 µL) disks were used as negative controls, while vancomycin was considered as a positive control. Plates were incubated at 37 °C for 24 h. All experiments were performed in triplicate. The halos were measured in millimeters using calipers.

In order to check the dissolving time of the tablets, the dissolving sequence was monitored every five minutes till complete dissolution.

### 2.6.3. Statistical Analysis

The disk diffusion results were statistically analyzed using one-way ANOVA followed by Tukey's HSD multiple comparisons of means using R (v. 3.5.1) [21]. Data are presented as boxplots. Differences were considered significant for  $p$ -values  $<$  0.05.

## 3. Results and Discussion

### 3.1. Material Preparation

A successful host–guest molecular inclusion was achieved via physical contact between the EOs and b-CD through sonication. The standard protocol requires a nearly stoichiometric 1:1 mixture of b-CD and EOs. This method was applied to both EOs and noteworthy temperature increases (till 60 °C) were observed alongside the treatment as a reasonable consequence of the molecular inclusion phenomena. After the treatment, the solid-state materials were separated from the residual oils, and the unreacted b-CD was re-

moved using water. In this context, small amounts of the cyclodextrin host were solubilized and removed, with the core of the solid product having a decreased water affinity.

### 3.2. FT-IR Spectroscopy

FT-IR spectra of the *S. montana* EO (blue profile), b-CD (red profile) and the solid-state beta-cyclodextrin-*S. montana* EO (b-CD-EO-S) mixture (green profile) are reported in Figure 1C. At  $1463\text{ cm}^{-1}$ , the peak of the EO was found in the b-CD-EO-S pattern, though not provided by the cyclodextrin pattern itself, which was featured as a broad shifted shoulder. At  $1057\text{ cm}^{-1}$ , a peak of the EO was observed in the b-CD-EO-S mixture profile. In this latter profile, a shouldered peak at  $1003\text{ cm}^{-1}$  was nearly coincident with a shoulder of the EO  $997\text{ cm}^{-1}$  peak, which was one of the most intense in the entire spectrum. The b-CD peak at  $938\text{ cm}^{-1}$  was convex, whilst it was observed to be concave in the b-CD-EO-S profile; moreover, the shoulder at  $936\text{ cm}^{-1}$  was nearly coincident with the EO peak at  $935\text{ cm}^{-1}$ . A strong EO peak at  $864\text{ cm}^{-1}$  was noticed in the b-CD-EO-S reacted mixture, while b-CD itself provided a signal at  $860\text{ cm}^{-1}$ . In the spectral range between  $827$  and  $770\text{ cm}^{-1}$ , the b-CD pattern was convoluted in the b-CD-EO-S profile. The peak at  $706\text{ cm}^{-1}$  was asymmetrical in the b-CD-EO-S pattern; it actually broadened toward  $720\text{ cm}^{-1}$ , where a rather intense EO peak occurred. The EO peak at  $697\text{ cm}^{-1}$  was distinctly noticed in the b-CD-EO-S reacted mixture profile. The  $640\text{ cm}^{-1}$  EO peak overlapped with the b-CD pattern in b-CD-EO-S; here, a shoulder found at  $594\text{ cm}^{-1}$  for a b-CD peak was correlated with the EO peak occurring at this frequency.

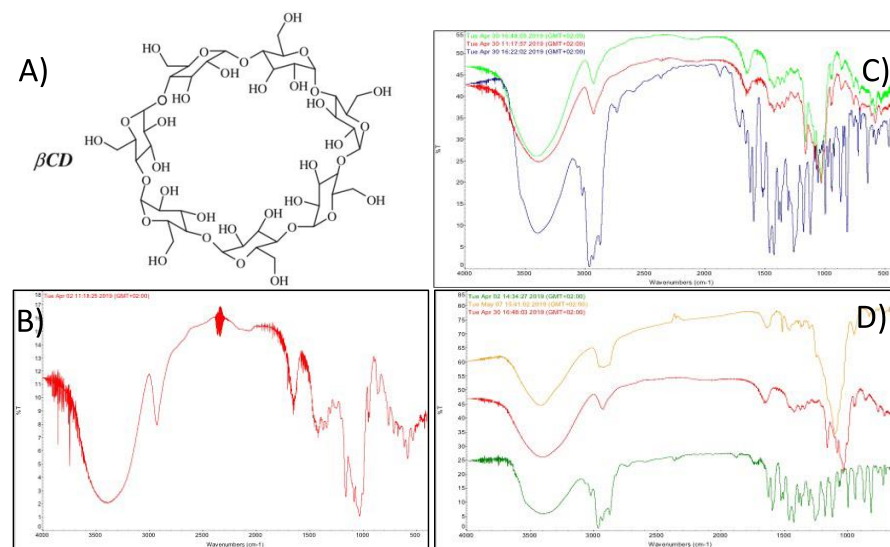


**Figure 1.** (A) b-CD chemical structure; (B) b-CD IR profile; (C) *S. montana* EO (blue), b-CD (red) and the reacted b-CD-EO solid-state mixture (green) IR profiles; (D) *T. capitatus* EO (green), b-CD (red) and the reacted b-CD-EO solid-state mixture (orange) IR profiles.

In Figure 1D, the spectra of the *T. capitatus* EO (green profile), b-CD (red profile) and the beta-cyclodextrin-*T. capitatus* EO reacted (b-CD-EO-T) solid-state mixture (orange profile) are reported. In the aliphatic C-H spectral stretching region, the EO components were observed. The strong EO peak at  $2964\text{ cm}^{-1}$  was shifted in the b-CD-EO-T mixture at  $2956\text{ cm}^{-1}$  (Figure 1D). Furthermore, the strong EO peak at  $2871\text{ cm}^{-1}$  was maintained in the b-CD-EO-T pattern. In this latter pattern, the diagnostic broad b-CD signal at  $1643\text{ cm}^{-1}$  was accompanied by a featured shoulder at  $1622\text{ cm}^{-1}$ , which also occurred in the EO profile. At  $1526\text{ cm}^{-1}$ , in the spectral region where C=C stretching modes mixed with related in-plane C-H bending modes of the different terpenoid molecules occurred, and a strong peak was observed in the EO pattern; this featured was then found in the b-CD-EO-T system, which had shifted to  $1515\text{ cm}^{-1}$ . The two strong EO peaks at  $1461$  and  $1423\text{ cm}^{-1}$  overlapped with the b-CD pattern in the b-CD-EO-T complex, with an inversion

of their relative spectral intensities. The EO feature at  $1385\text{ cm}^{-1}$  inside the alcoholic C–OH bending region was maintained in the b-CD–EO–T complex. At  $1366\text{ cm}^{-1}$ , the observed b-CD–EO–T peak displayed a bandwidth that was correlated with the spectral feature that was noticed in the same region in the EO pattern. It is noteworthy that the EO shoulder at  $1347\text{ cm}^{-1}$  was observed at  $1351\text{ cm}^{-1}$  in the b-CD–EO–T mixture with a strong spectral intensity. Both the b-CD and EO profiles set a peak at  $1304\text{ cm}^{-1}$ , which was then observed shifted to  $1300\text{ cm}^{-1}$  in the b-CD–EO–T system. Moreover, the strong EO peak at  $1256\text{ cm}^{-1}$  was shifted to  $1247\text{ cm}^{-1}$  in the b-CD–EO–T complex. In the same complex pattern, the  $1188\text{ cm}^{-1}$  peak was ascribed to the parent EO feature. The minimum transmittance frequency in the b-CD–EO–T profile at  $1101\text{ cm}^{-1}$  was correlated with the strong shifted peak occurring in the EO at  $1118\text{ cm}^{-1}$ . The paired EO peaks at  $1070$  and  $1058\text{ cm}^{-1}$  were correlated with the broadened shoulder of the main b-CD spectral feature at  $1066\text{ cm}^{-1}$  in the b-CD–EO–T system. A strong EO  $1000\text{ cm}^{-1}$  peak was noticed in the b-CD–EO–T profile in the indented shoulder of the main spectral feature, which occurred at  $1008\text{ cm}^{-1}$ . The b-CD–EO–T at  $948\text{ cm}^{-1}$  was the resulting overlap of the  $950$  and  $938\text{ cm}^{-1}$  peaks, which were added to the strong EO peak that occurred at  $938\text{ cm}^{-1}$ . It is worth noting that the two strong EO peaks at  $870$  and  $814\text{ cm}^{-1}$ , which were correlated with the gamma-C–H out-of-plane vibrations of the abundant aromatic components, were severely hampered in the b-CD–EO–T pattern, providing small broadened features at  $831$  and  $806\text{ cm}^{-1}$ . The b-CD  $614\text{ cm}^{-1}$  peak was extinguished in the complex, while the  $579\text{ cm}^{-1}$  was maintained and possibly overlapped with the EO  $575\text{ cm}^{-1}$  peak. The EO peak at  $468\text{ cm}^{-1}$  was greatly enhanced and broadened in the b-CD–EO–T mixture at  $470\text{ cm}^{-1}$  (Figure 1D).

In both reacted mixtures, the observed spectral shifts were comprehensively higher than the applied  $2\text{ cm}^{-1}$  spectral resolution; however, the  $1\text{ cm}^{-1}$  high-resolution FT-IR spectra were obtained to support and corroborate the reported results.

Analysis of the IR spectral profile of the reacted b-CD–EO solid-state mixture supported the actual molecular inclusion phenomena of different oil components inside the lipophilic folder of b-CD. By comparison with the IR patterns of the single separated components, general broadening of signals accompanied by different relative spectral intensities were noticed for both reacted systems, with the spectra not being a mere superposition of the parent patterns [22]. In previous studies, these observed comprehensive spectral scenarios were established as being correlated with host–guest molecular encapsulation and the subsequent molecular complex formation [22,23].

### 3.3. Chromatographic and Mass Spectrometric Characterization

ESI-MS spectra were recorded for the b-CD and solid-state b-CD–EO reacted mixtures. The ESI-MS analyses qualitatively supported the successful formation of b-CD inclusion complexes with both the EOs. In fact, the characteristic  $m/z$  values were found both in the oils and the solid products based on cyclodextrin indicating that several components of the oil were actually included in the saccharide host (Figures 2 and 3). Tentative assignments of the fragment structures were performed and terpene fragments were identified, but only from the ESI-MS data; it was difficult to unambiguously attribute the observed signals to specific terpene structures.

From this perspective, the same samples employed for the ESI-MS analysis were subjected to GC-MS chromatographic analysis, with the aim of investigating the included components. In Figures 4 and 5, the relative chromatograms are reported.

Some peaks that were found in the EOs were also identified in the solid-state b-CD–EO complexes, confirming the successful formation of b-CD–EO complexes with both EOs. In more detail, the molecules that are reported in the literature to exert a biological function or are typical of the EOs are listed in Tables 1 and 2. These molecules were found both in the EOs and in the relative inclusion samples.

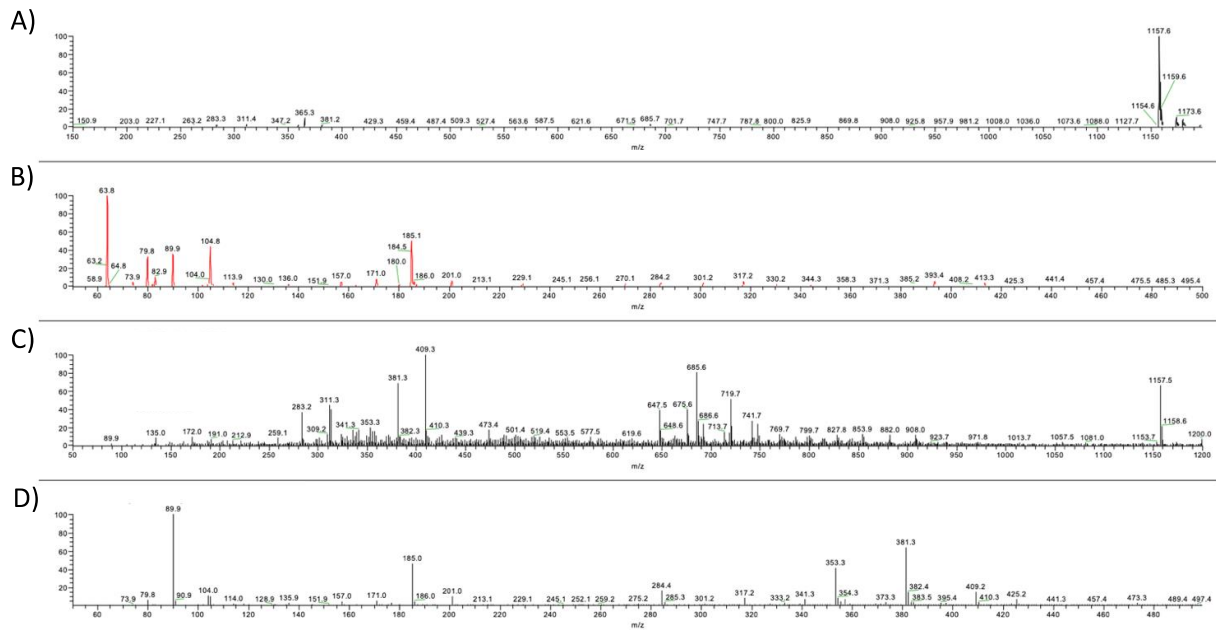


**Figure 2.** ESI-MS spectra of (A) b-CD, (B) *S. montana* EO, (C) solid-state b-CD-EO-S in the high mass range and (D) solid-state b-CD-EO-S in the low mass range.

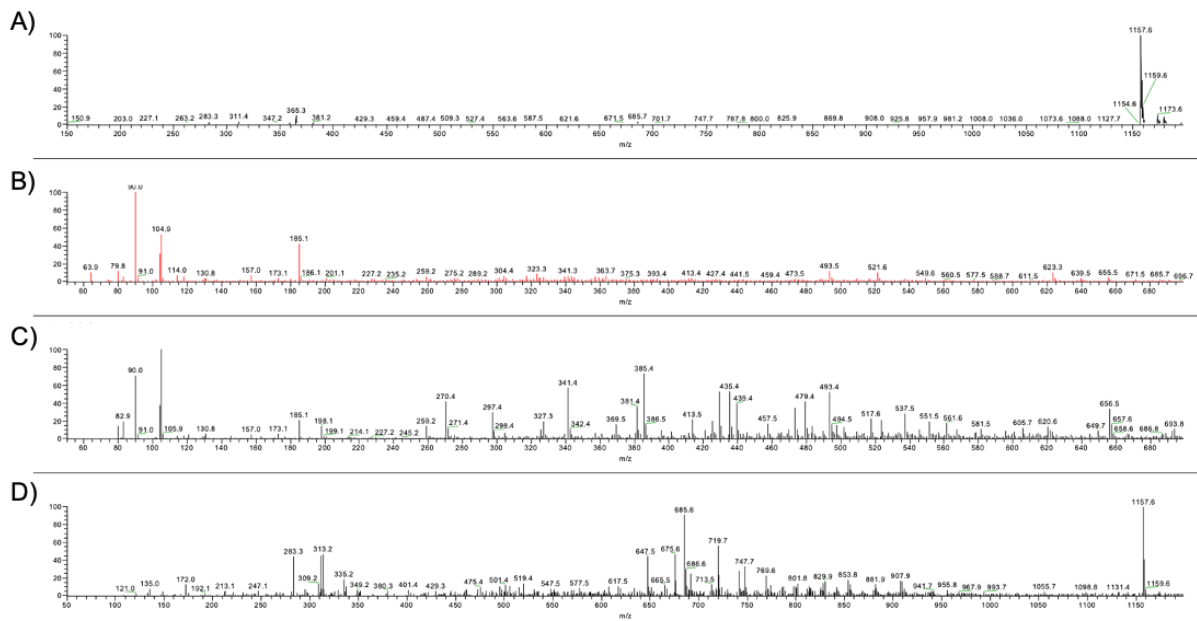
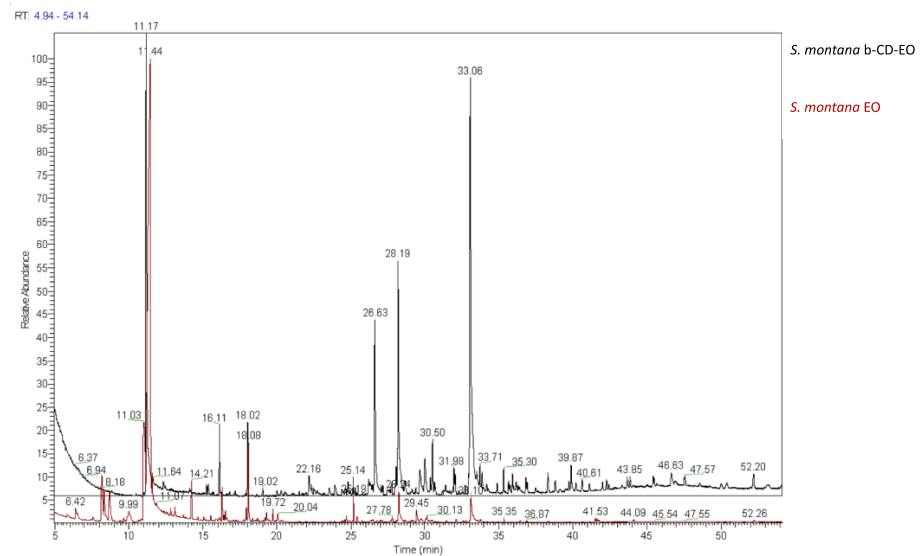


**Figure 3.** ESI-MS spectra of (A) b-CD, (B) *T. capitatus* EO b-CD, (C) solid-state b-CD-EO-T in the high mass range and (D) solid-state b-CD-EO-T in the low mass range.

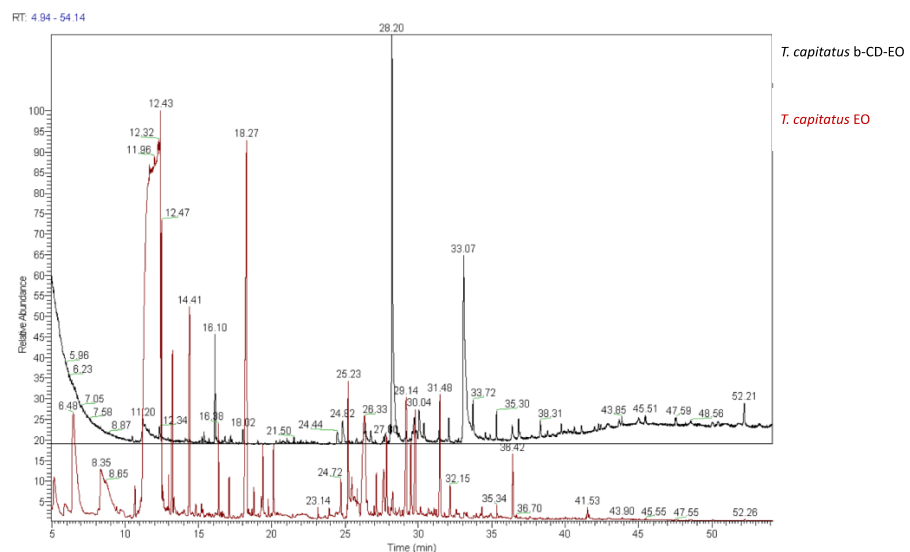
### 3.4. Synthesis of the Pharmaceutical b-CD-EO Tablet

Figure 6 shows the different steps of the tablet preparation procedure. Tablets were successfully produced in a replicable way. The produced tablets showed characteristics that were similar to pharmaceutical ones. In particular, they presented the same compactness and stability for both EOs, suggesting that their formulation was transversal for EOs of different compositions. Tablets were also stored for sixty days at room temperature and showed no change in their appearance, compactness or antimicrobial performances. The production of a solid tablet solved the problem of administering EO for the treatment of both oral and vaginal infections. In order to understand whether the efficacy of these

tablets was comparable to that of the related pure EO, comparative validation with agar diffusion tests were performed.



**Figure 4.** GC-MS chromatograms of *S. montana* EO (red line) and solid-state b-CD-EO-S (black line) samples.



**Figure 5.** GC-MS chromatograms of *T. capitatus* EO (red line) and *T. capitatus* solid-state b-CD-EO-T (black line) samples.

### 3.5. Antifungal and Antibacterial Assays

Figure 7 shows the results of the antifungal and antibacterial activity assays of the EOs extracted from *S. montana* and *T. capitatus* in both pure EO and tablet forms. Data obtained using disk diffusion assays on two *Candida* reference strains and one *S. aureus* reference strain showed that both EOs and the tablets had antifungal and antibacterial activities that were significantly higher (2–3-fold) than the reference drugs used as positive controls (clotrimazole and vancomycin, respectively). The b-CD host exerted no biological activity against the tested microorganisms (data not shown). The tablet formulation induced a significant decrease in antifungal and antibacterial efficacy compared to the corresponding pure EO. However, the tablet was more effective than the reference antifungal and/or antibiotic drugs. The difference in effectiveness between the tablets and pure EOs was more evident for yeasts than for *S. aureus*, thus showing a different response to the tablet dissolv-

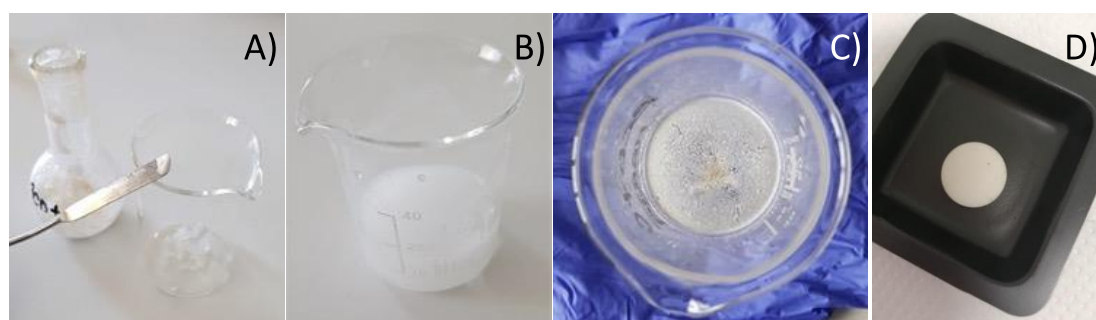
ing time. Moreover, these different effects may have been due to the different effectiveness of the active components of the oil that are found inside the b-CD-EO and therefore inside the tablet. These components could have a different cellular target and hence display lower performance against yeasts than in the tested strain. It must be emphasized that the results obtained regarding growth inhibition of the tested microorganisms by pure EOs is consistent with our previous works [16–19].

**Table 1.** Molecules found in both the *S. montana* EO and the relative tablet that show a biological function or are typical of this EO.

Molecules	CAS Number	T <sub>rit</sub>	<i>S. Montana</i> EO	<i>S. Montana</i> EO + b-CD	Effects
Carvacrol	499-75-2	12.43	X	X	Antibacterial
1-Hydroxy-4-methyl-2,6-di-tert-butyl benzene (BHT)	128-37-0	16.1	X	X	Antioxidant
Caryophyllene oxide	1139-30-6	18.27	X	X	Relaxant effects, analgesic, tumor-suppressing agent
Decalin, 1-methoxymethyl	4645-15-2	24.66	X	X	EOs constituent
Heneicosane	629-94-7	30.36	X	X	
1-Octadecanol	112-92-5	30.5	X	X	
Tricosane	638-67-5	33.06	X	X	
9-Octadecenamide (oleamide)	301-02-0	39.73	X	X	EOs constituent

**Table 2.** Molecules found in both the *T. capitatus* EO and the relative tablet that show a biological function or are typical of this EO.

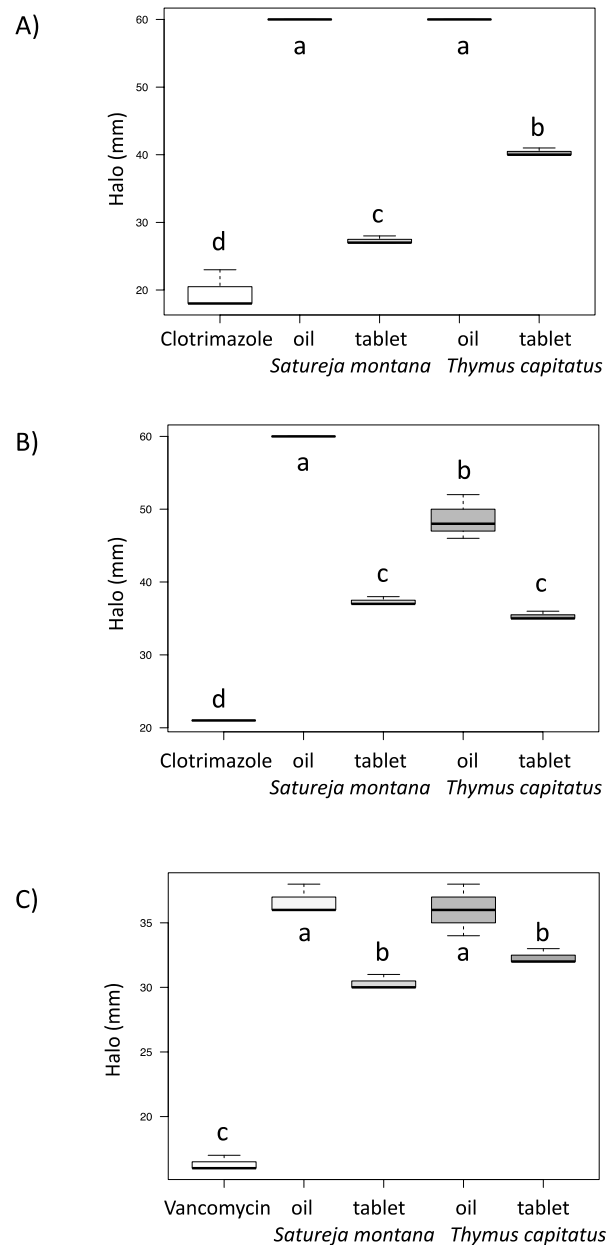
Molecules	CAS Number	T <sub>rit</sub>	<i>T. Capitatus</i> EO	EO + b-CD	Effects
Thymol	89-83-8	11.20	X	X	Antibacterial and antifungal antibacterial
Carvacrol	499-75-2	12.43	X	X	
Isoascaridole	512-85-6	12.47	X	X	
1-1-Hydroxy-4-methyl-2,6-di-tert-butyl benzene (BHT)	128-37-0	16.1	X	X	Antioxidant
Caryophyllene oxide	1139-30-6	18.27	X	X	Relaxant effects, analgesic, tumor suppressing agent
Heptadecanitrile	5399-02-0	24.82	X	X	Plant Metabolite
Oleanitrile	112-91-4	28.20	X	X	
Tricosane	638-67-5	32.08	X	X	
9-Octadecenamide (oleamide)	301-02-0	33.07	X	X	Cannabinoid mimic



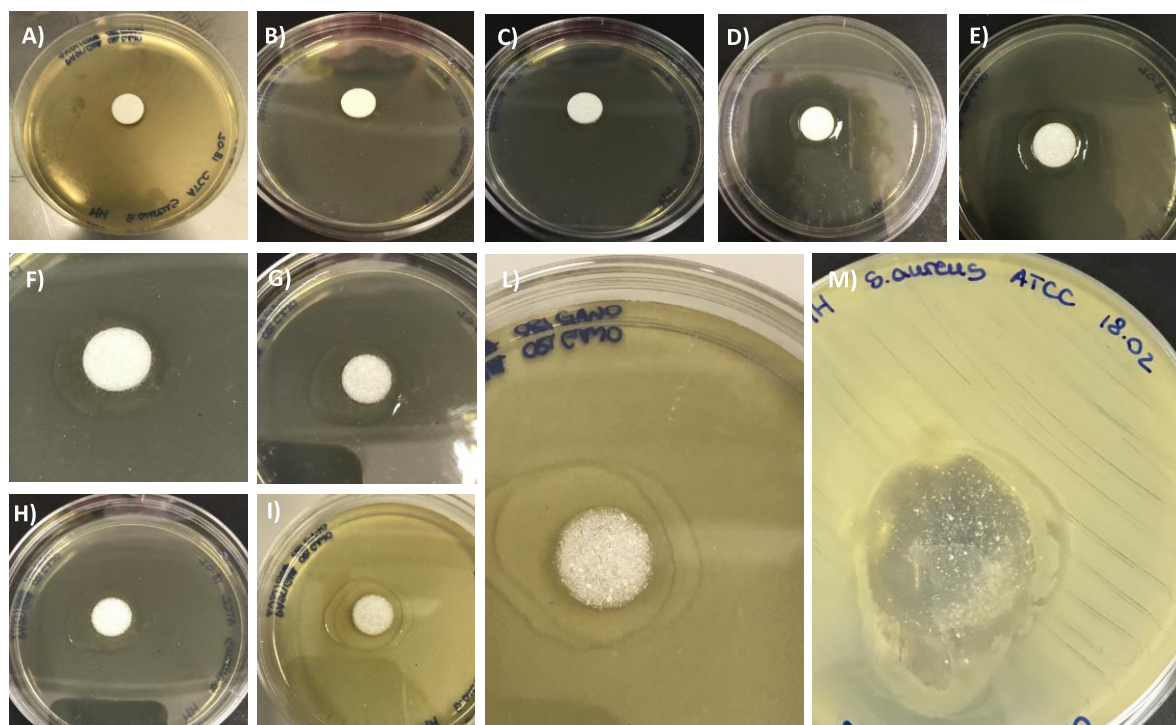
**Figure 6.** Tablet preparation steps. (A–C) b-CD-EOs powder mixtures embedded in polyvinylpyrrolidone (PVP). (D) The obtained solid-state composite powder was pressed in order to obtain 1 cm diameter round tablets.

Figure 8 shows the dissolving sequence of the tablets. Once in contact with the medium contained in the Petri dish, the tablet began to solve, and about 1 h later, it was almost completely dissolved. After 24 h, at the end of the incubation time, it was completely dissolved. The prolonged dissolving time of the tablet could be a limit in the interpretation of the in vitro test. However, from an applicative point of view, a long dissolving time means an increased exposure time of the patient to the bioactive substance and therefore

a greater possibility of efficacy in inhibiting the growth of pathogenic microorganisms. Potential applications of this tablet in daily practice could be as a chewable tablet for oral infections or as a vaginal tablet. In both cases, a prolonged dissolving time favors a gradual administration of EOs. In fact, the pure EOs may have a mildly inflammatory effect given by the mild cytotoxicity demonstrated in previous works [17]; the slow release that is mediated by the tablet form could reduce this potential side effect.



**Figure 7.** Disk diffusion assay. The halo diameters (mm) were recorded using calipers. Two EOs extracted from *S. montana* and *T. capitatus* were tested as both pure oils or as tablets. Clotrimazole and vancomycin were used as positive controls. (A) *C. albicans* ATCC 14053, (B) *C. glabrata* ATCC 15126 and (C) *S. aureus* NCTC 6571. Different letters above the boxes indicate significant differences according to one-way ANOVA followed by Tukey's HSD test ( $p < 0.05$ ).



**Figure 8.** Tablet dissolving sequence. From (A–L) photographs were acquired every 5 min. The last picture (M) was taken 24 h after the first one (A), at the end of the incubation time.

#### 4. Conclusions

In conclusion, different molecular components of two strongly antimicrobial EOs that were extracted from *S. montana* and *T. capitatus* were successfully included as host-guest complexes in b-CD. The obtained inclusion materials could be pelleted as proto-pharmaceutical tablets in a PVP matrix while retaining the comprehensive antifungal and antibacterial performances that featured regarding both the applied parent oils. Chemical characterization using FT-IR spectroscopy, ESI-MS spectrometry and GC-MS analysis ascertained the actual encapsulation inside the cyclodextrin lipophilic folders of different specific terpenoid and aromatic moieties that ensured biocidal responses that were similar to those provided by conventional pharmaceutical antibiotics.

The obtained experimental result was deemed noteworthy, paving the way for the first use of solid-state controlled-release pharmaceutical applications of EOs in antifungal and antibacterial treatments.

**Author Contributions:** Conceptualization, A.A.; methodology, A.A.; formal analysis, A.A., A.C. (Alice Caramaschi), A.C. (Alessia Cattaneo), G.N., M.M. and V.G.; data curation, N.M.; writing—original draft preparation, A.A., E.B., N.M. and V.G.; writing—review and editing, A.A., E.B., N.M., V.G., G.N. and E.G. All authors read and agreed to the published version of the manuscript.

**Funding:** This research received no external funding.

**Institutional Review Board Statement:** Not applicable. This study did not involve humans or animals.

**Informed Consent Statement:** Not applicable.

**Acknowledgments:** Flora s.r.l. (Pisa, Italy) is acknowledged for the loan of *T. capitatus* and *S. montana* essential oils. The authors want to thank Marianna Farotto (DiSIT, Vercelli, Italy) for her kind assistance in biological tests.

**Conflicts of Interest:** The authors declare no conflict of interest.

## References

1. Adalja, A.A.; Watson, M.; Toner, E.S.; Cicero, A.; Inglesby, T.V. Characteristics of Microbes Most Likely to Cause Pandemics and Global Catastrophes. In *Global Catastrophic Biological Risks*; Inglesby, T.V., Adalja, A.A., Eds.; Springer International Publishing: Cham, Switzerland, 2019; Volume 424, pp. 1–20. ISBN 978-3-030-36310-9.
2. Sofi, M.S.; Hamid, A.; Bhat, S.U. SARS-CoV-2: A critical review of its history, pathogenesis, transmission, diagnosis and treatment. *Biosaf. Health* **2020**, *2*, 217–225. [[CrossRef](#)] [[PubMed](#)]
3. World Health Organization (Ed.) *Health21: The Health for All Policy Framework for the WHO European Region*; European health for all series; World Health Organization, Regional Office for Europe: Copenhagen, Denmark, 1999; ISBN 978-92-890-1349-9.
4. Atanasov, A.G.; Zotchev, S.B.; Dirsch, V.M.; Supuran, C.T. Natural products in drug discovery: Advances and opportunities. *Nat. Rev. Drug Discov.* **2021**, *20*, 200–216. [[CrossRef](#)] [[PubMed](#)]
5. Lahlou, M. The Success of Natural Products in Drug Discovery. *Pharmacol. Pharm.* **2013**, *04*, 17–31. [[CrossRef](#)]
6. Shabbir, M.A.B.; Shabbir, M.Z.; Wu, Q.; Mahmood, S.; Sajid, A.; Maan, M.K.; Ahmed, S.; Naveed, U.; Hao, H.; Yuan, Z. CRISPR-cas system: Biological function in microbes and its use to treat antimicrobial resistant pathogens. *Ann. Clin. Microbiol. Antimicrob.* **2019**, *18*, 21. [[CrossRef](#)] [[PubMed](#)]
7. Kummerer, K. Significance of antibiotics in the environment. *J. Antimicrob. Chemother.* **2003**, *52*, 5–7. [[CrossRef](#)] [[PubMed](#)]
8. Wright, G.D. The antibiotic resistome: The nexus of chemical and genetic diversity. *Nat. Rev. Microbiol.* **2007**, *5*, 175–186. [[CrossRef](#)] [[PubMed](#)]
9. World Health Organization (Ed.) *Antimicrobial Resistance: Global Report on Surveillance*; World Health Organization: Geneva, Switzerland, 2014; ISBN 978-92-4-156474-8.
10. Alekshun, M.N.; Levy, S.B. Molecular Mechanisms of Antibacterial Multidrug Resistance. *Cell* **2007**, *128*, 1037–1050. [[CrossRef](#)] [[PubMed](#)]
11. Erickson, K.E.; Otoupal, P.B.; Chatterjee, A. Transcriptome-Level Signatures in Gene Expression and Gene Expression Variability during Bacterial Adaptive Evolution. *mSphere* **2017**, *2*. [[CrossRef](#)] [[PubMed](#)]
12. Antinori, S.; Milazzo, L.; Sollima, S.; Galli, M.; Corbellino, M. Candidemia and invasive candidiasis in adults: A narrative review. *Eur. J. Intern. Med.* **2016**, *34*, 21–28. [[CrossRef](#)] [[PubMed](#)]
13. Adorjan, B.; Buchbauer, G. Biological properties of essential oils: An updated review. *Flavour Fragr. J.* **2010**, *25*, 407–426. [[CrossRef](#)]
14. Bakkali, F.; Averbeck, S.; Averbeck, D.; Idaomar, M. Biological effects of essential oils—A review. *Food Chem. Toxicol.* **2008**, *46*, 446–475. [[CrossRef](#)] [[PubMed](#)]
15. Raut, J.S.; Karuppaiyil, S.M. A status review on the medicinal properties of essential oils. *Ind. Crops Prod.* **2014**, *62*, 250–264. [[CrossRef](#)]
16. Bona, E.; Massa, N.; Novello, G.; Pavan, M.; Rocchetti, A.; Berta, G.; Gamalero, E. Essential oil antibacterial activity against methicillin-resistant and -susceptible *Staphylococcus aureus* strains. *Microbiol. Res. (Pavia)* **2019**, *10*. [[CrossRef](#)]
17. Bona, E.; Cantamessa, S.; Pavan, M.; Novello, G.; Massa, N.; Rocchetti, A.; Berta, G.; Gamalero, E. Sensitivity of *Candida albicans* to essential oils: Are they an alternative to antifungal agents? *J. Appl. Microbiol.* **2016**, *121*, 1530–1545. [[CrossRef](#)] [[PubMed](#)]
18. Massa, N.; Cantamessa, S.; Novello, G.; Ranzato, E.; Martinotti, S.; Pavan, M.; Rocchetti, A.; Berta, G.; Gamalero, E.; Bona, E. Antifungal activity of essential oils against azole-resistant and azole-susceptible vaginal *Candida glabrata* strains. *Can. J. Microbiol.* **2018**, *64*, 647–663. [[CrossRef](#)]
19. Bona, E.; Arrais, A.; Gema, L.; Perotti, V.; Birti, B.; Massa, N.; Novello, G.; Gamalero, E. Chemical composition and antimycotic activity of six essential oils (cumin, fennel, manuka, sweet orange, cedar and juniper) against different *Candida* spp. *Nat. Prod. Res.* **2019**, 1–6. [[CrossRef](#)]
20. Clericuzio, M.; Hussain, F.H.S.; Amin, H.I.M.; Bona, E.; Gamalero, E.; Giorgia, N.; Lappano, R.; Talia, M.; Maggiolini, M.; Bazzicalupo, M.; et al. Cytotoxic, Anti-bacterial, and Wound-healing Activity of Prenylated Phenols from the Kurdish Traditional Medicinal Plant *Onobrychis Carduchorum* (Fabaceae). *Planta Medica. Int. Open* **2020**, *07*, e106–e113. [[CrossRef](#)]
21. R Core. *R: A Language and Environment for Statistical Computing*; R foundation for statistical computing: Vienna, Austria, 2018.
22. Parlati, S.; Gobetto, R.; Barolo, C.; Arrais, A.; Buscaino, R.; Medana, C.; Savarino, P. Preparation and application of a  $\beta$ -cyclodextrin-disperse/reactive dye complex. *J. Incl. Phenom. Macrocycl. Chem.* **2007**, *57*, 463–470. [[CrossRef](#)]
23. Arrais, A.; Savarino, P. Raman spectroscopy is a convenient technique for the efficient evaluation of cyclodextrin inclusion molecular complexes of azo-dye colorants and largely polarisable guest molecules. *J. Incl. Phenom. Macrocycl. Chem.* **2009**, *64*, 73–81. [[CrossRef](#)]